for cell survival curves. The relative biological effectiveness (RBE) for neutron beams was obtained as the ratio of the mean value of D_{10} to that of gamma rays.

Gamma-H2AX focus assay

A Gamma-H2AX focus assay was performed to detect DNA double-strand breaks (DSBs) [16]. Cells were poured onto 22 × 22 mm coverslips in 35 mm dishes filled with medium and placed in an incubator for the stated repair time after irradiation. Briefly, cells were fixed with 4% paraformaldehyde in phosphate-buffered saline (PBS), permeabilized for 10 min on ice in 0.5% Triton X-100 in PBS, washed thoroughly with PBS, and then blocked for 1 h with 3% skim milk in PBS. The coverslips were then incubated with an antibody against histone H2AX phosphorylated on serine 139 (Upstate Biotechnology, Lake Placid, NY) for 2 h at 37°C. After incubation with primary antibody, the cells were washed with PBS, and Alexa Fluor 488-labeled anti-mouse IgG secondary antibodies (Invitrogen) were added. The coverslips were incubated for 1 h at 37°C, washed with PBS, and sealed onto glass slides with 0.05 ml PBS containing 10% glycerol (Wako, Osaka, Japan) and 20 μg/ml DAPI (4'6-diamidino-2-phenylindole; Invitrogen). The cells were examined using a Keyence fluorescence microscope (Keyence, Osaka, Japan), and the green intensity of the phosphor-H2AX signal on digitized images was automatically analyzed using the software package Dynamic Cell Count (Keyence). Using this software package, the numbers and sizes of foci exhibiting high-intensity staining with gamma-H2AX (green) in each type of A172 cell population were determined in more than 100 areas per condition.

Statistical analysis

Values are presented as means ± standard errors. Statistical analyses were performed using the unpaired, two-tailed Student's *t*-test. A significance level of $P < 0.05$ was used for all analyses. The data on cell survival were fitted to the linear-quadratic dose relationship.

RESULTS

Detection of stemness in GSLCs

Figure 1 shows the characteristics of the GSLCs. To induce GSLCs, we cultured the A172 cells in SFM, as described above. Seven days after culturing in SFM, these cells were form-floating, neurosphere-like spheroid cells (Fig. 1A). In the Western blotting analysis, we found that two neural stem cell markers, Sox2 and Musashi, were more highly expressed in the GSLCs than in the A172 cells cultured in serum-containing medium as control cells (CCs) (Fig. 1B). However, no apparent CD133 expression was detected in either GSLCs or CCs that were cultured for 7 d. Therefore, we changed the CD133-detection assay for FACS analysis by using several time-points. In the FACS analysis, the ratio of CD133-positive GSLCs increased by 9% after 14 d, whereas the ratio of CD133-positive CCs was unchanged (Fig. 1C). The FACS analysis confirmed marked positivity in the WERI-Rb-1 (WE) cells, a retinoblastoma cell line used as a control (data not shown).

Radiosensitivity of GSLCs and CCs

The radiosensitivity of GSLCs was compared with that of CCs under gamma-ray or neutron-beam irradiation. Figure 2 shows the surviving fractions of A172 under the two culture conditions after gamma-ray or neutron-beam irradiation. After gamma-ray irradiation, GSLCs showed significantly greater radioresistance than CCs. On the other hand, after neutron-beam irradiation, there was no significant difference in the sensitivity between GSLCs and CCs. The D_{10} values were calculated by linear regression analysis from the survival curves shown in Fig. 2, and the D_{10} dose parameters for survival following irradiation and their RBEs are listed in Table 1. The D_{10} value represents the radiation dose that produces a survival fraction of 10%. To examine the difference in radiosensitivity between GSLCs and CCs, we referred to the resistance ratio. This ratio was calculated from the D_{10} dose of GSLCs per that of each respective CC by these two forms of irradiation. For example, under gamma-ray irradiation, the ratio of the D_{10} dose of GSLCs to that of CCs was 3.98/3.02 = 1.318. On the other hand, under neutron-beam irradiation, the D_{10} dose of GSLCs per that of CCs was 1.17/1.25 = 0.936. The resistance ratio of neutron beams was smaller than that of gamma rays. Consequently, neutron-beam irradiation overcame the resistance to gamma-ray irradiation in A172 GSLCs. In other words, these results suggested that A172 GSLCs, which were radioresistant to gamma rays, became sensitive to neutron beams.

Persistence of gamma-H2AX foci following irradiation

Figure 3 shows representative images of each type of A172 cells at 24 h after each type of irradiation. The fluorescence intensity of gamma-H2AX foci produced by neutron beams was stronger than that produced by gamma rays in both GSLCs and CCs, under the same staining conditions and the same photographic exposure time (Fig. 3). At a glance, the foci in both CCs and GSLCs produced by neutrons seemed larger than those produced by gamma rays. Figure 4A and B show the change in the numbers of gamma-H2AX foci following 4 Gy of gamma-ray or neutron irradiation in GSLCs and CCs induced from A172 cells. There were significantly more gamma-H2AX foci per cell in CCs than in GSLCs 24 h after gamma-ray irradiation. However, after neutron-beam irradiation, there was no apparent difference between GSLCs and CCs in the number of gamma-H2AX foci. Figure 4C and D show the distribution histograms of the size of foci induced in GSLCs and CCs, respectively, and Fig. 4E shows the mean size of gamma-H2AX foci at 24 h post-irradiation,

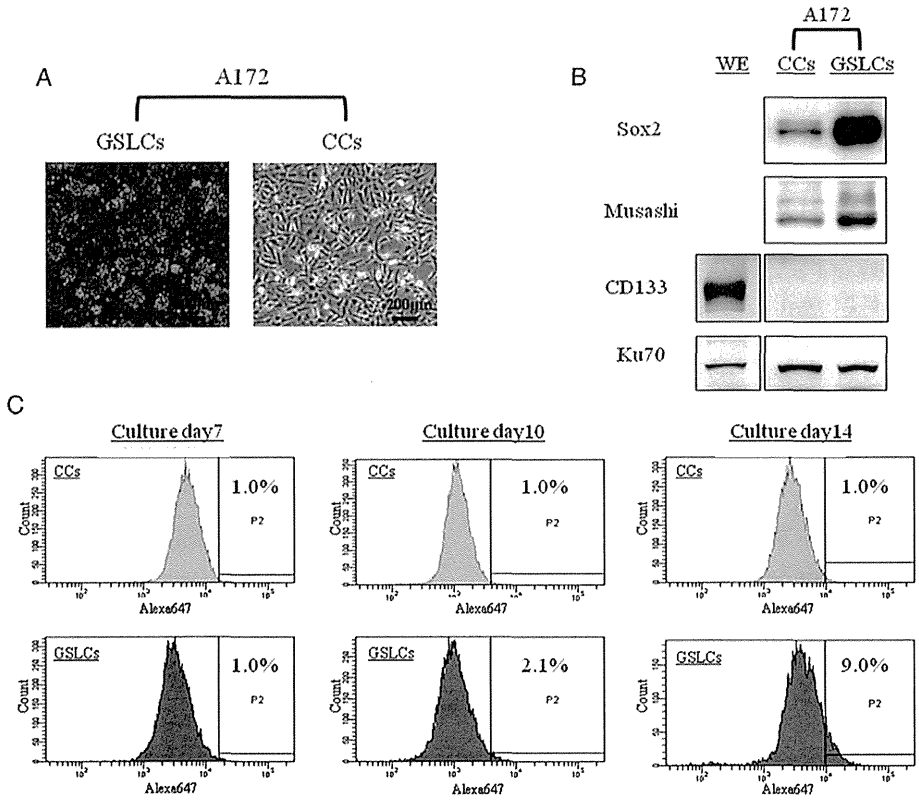

Fig. 1. Characteristics of the glioma stem-like cells. (**A**) The morphology of human glioma cell line A172 cultured for 7 d in serum-containing medium or serum-free medium. (**B**) The expression of typical stem cell marker proteins as examined by Western blot assays on Day 7 after culture. (**C**) The ratio of CD133-positive cells in FACS analysis; the number of days of culture is shown in each column, and the rate of CD-133-positive GSLCs was measured with a cutoff value obtained from the fluorescence intensity that occupied 1% by putative CD133-positive CCs in the total population. GSLCs = glioma stem-like cells; CCs: control cells; WE = WERI-Rb-1 (the retinoblastoma cell line used as a positive control for anti-CD133 Ab).

measured using the BZII image analysis system (Keyence). Figure 4C, D and E reveal definitively that neutron-beam irradiation induced larger gamma-H2AX foci than those observed after gamma-ray irradiation, not only in CCs but also in GSLCs of A172 cells. These results might suggest that DSBs were repaired more efficiently in GSLCs than in CCs following gamma-ray irradiation. In contrast, under neutron irradiation, the DNA DSBs were not repaired efficiently in either GSLCs or CCs.

DISCUSSION

Research on GSCs has been conducted for many years, and GSCs have been found to contribute to the recurrence and resistance to therapy of malignant gliomas [2–6]. The difficulty of treating GBM may be attributed to the existence of GSCs in GBM, judging from the numerous published findings about GSCs.

In previous reports, GSCs were isolated from glioma tissues as spheres cultured in SFM containing stem-cell mitogens, epidermal growth factor and fibroblast growth factor, which is the same method used to isolate neural stem cells from brain tissue [2–4, 17]. Because of the lack of serum and the low plating density, most of the cells die, except those that divide in response to the stem-cell mitogens. The growth-factor-responsive cells proliferate to form floating clusters called neurospheres [18]. In this study, we induced GSLCs from cells of the human GBM line A172 using the same isolation-GSCs method as described previously [12]. In SFM containing the stem-cell mitogens, GSLCs were produced as neurosphere-like spheroid cells, and expressed neural stem cell markers such as Sox2 and Musashi (Fig. 1A and B) on Day 7 after induction. Actually, CD133 was hardly detected in Western blot analysis after 7 d of culture. Therefore, we performed FACS analyses and determined the ratio of CD133 positivity between GSLCs and CCs by kinetics study. The CD133-positive fraction in GSLCs

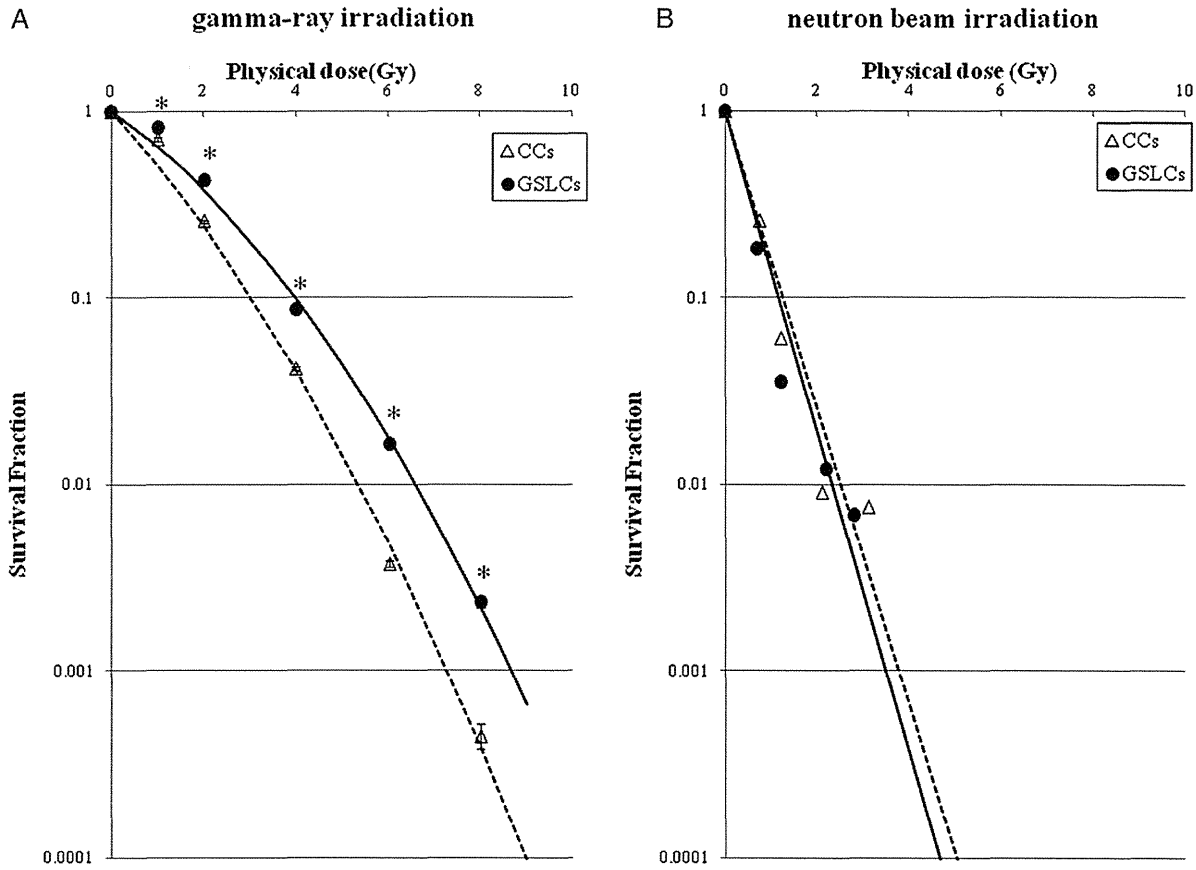

Fig. 2. Cell survival curves of GSLCs induced from A172 cells cultured with serum-free medium and CCs cultured with normal medium after gamma-ray (**A**), or neutron-beam irradiation (**B**). The data are fitted with a linear quadratic model. Bars represent the standard errors based on three independent experiments. $^*P < 0.05$ compared with the survival fraction of GSLCs and CCs. GSLCs = glioma stem-like cells; CCs = control cells.

Table 1. D_{10} physical dose and RBE (relative biological effectiveness)

	Irradiation	
(CCs)	**gamma rays**	**neutron beams**
D_{10} physical dose	3.02	1.25
RBE[a]		2.42
(GSLCs)		
D_{10} physical dose	3.98	1.17
RBE		3.40
Resistance ratio[b] (GSLCs/CCs)	1.318	0.936

[a]The ratio of the D_{10} physical dose compared to that of gamma rays. [b]The ratio of the dose of radiation necessary to obtain the D_{10} endpoint from GSLCs to that necessary in CCs. GSLCs = glioma stem-like cells, CCs = control cells, D_{10} = the radiation dose that produces a surviving fraction of 10%.

increased gradually in comparison with that in CCs day by day, and on Day 14, 9% of GSLCs were CD133-positive, although many GSLCs were still negative for CD133. In addition, 30 d of induction culture resulted in a higher percentage of CD133-positive GSLCs—up to 21% (data not shown). We speculate that it took a long time for CD133-positive cells to be refined in the SFM, and thus there was an insufficient number of CD133-positive cells for detection by Western blot analysis on Day 7. Indeed, CD133 positivity in our GSLCs from A172 on Day 7 was still small in number, but other stemness markers increased compared with CCs, and CD133 is not always a good GSC marker [19–21]. In addition, GSLCs induced by this method showed the upregulation of ATP-binding cassette transporter G2 and increased chemo-resistance in comparison with CCs (data not shown and manuscript in preparation). Above all, these GSLCs from A172 were somewhat radioresistant for low-LET gamma rays. Thus, we judged that these GSLCs were adequate for our further experiments. In any event, GSLCs had some degree of stemness. Actually, we tried to induce GSLCs from three GBM lines. Among them, GSLC from A172 was most prominent with GSC phenotype and apparent radioresistance to low-LET γ-rays. Thereafter, we used GSLCs from A172 in the current studies. We assessed the radiosensitivity of GSLCs using colony-forming assay on

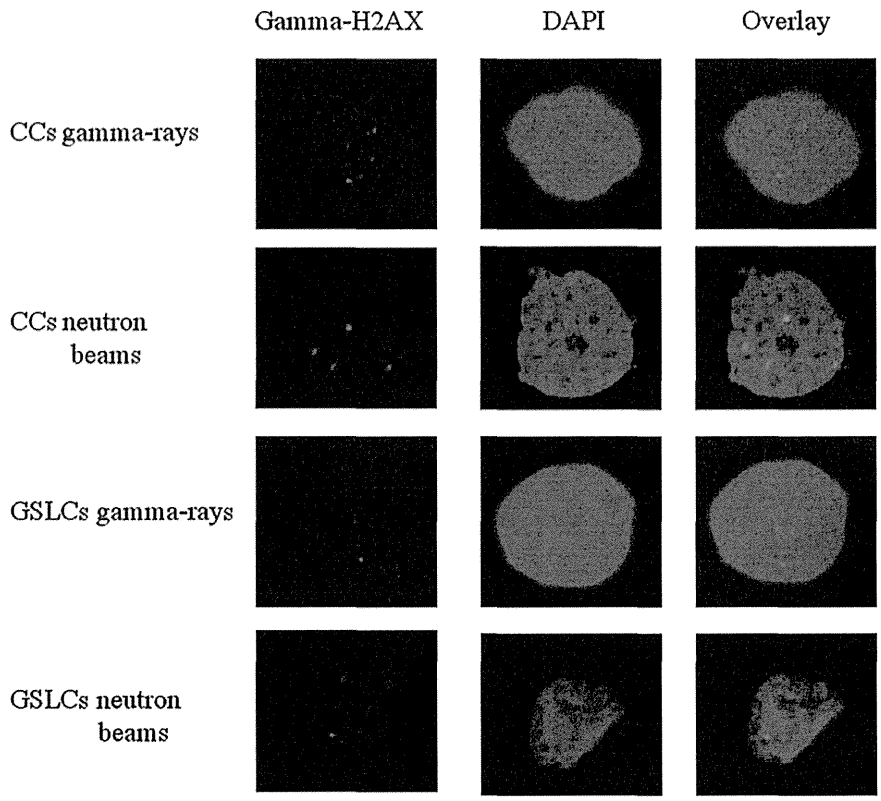

Fig. 3. Representative images of nuclear gamma-H2AX foci of CCs and GSLCs in A172. These cells were irradiated with different types of beams (total physical dose = 4 Gy) and fixed at 24 h post-irradiation for gamma-H2AX detection. DAPI = staining of nuclear DNA; Gamma-H2AX = staining of gamma-H2AX foci; GSLCs = glioma stem-like cells; CCs = control cells.

Day 7. Although, there might be a possibility of change in radiosensitivity associated with change of expression of CD133, especially in the later period of the induction of GSLCs, such as on Day 28, in the previous report [22], A172 CCs did not express CD 133, while radiation-induced GSLCs of A172 cells did express CD133. This is in accord with our experiment.

To evaluate the difference in radiosensitivity between GSLCs and CCs, we irradiated these cells with gamma rays or neutron beams, and found that the latter could overcome the radioresistance of GSLCs to gamma rays (Fig. 2 and Table 1). To obtain neutron beams, we used the Heavy Water Column of the KUR. These neutron beams consisted of fast, epithermal and thermal neutrons. Each neutron beam produced proton particles by elastic scattering ($^{1}H(n,n)^{1}H$) or nitrogen capture reaction ($^{14}N(n,p)^{14}C$) at irradiation, and these particles exhibited high-LET radiation. The LET of proton particles produced by the former reaction was about 50 keV/μm, and that produced by the latter reaction was about 35 keV/μm, whereas the gamma rays exhibited low-LET radiation. Therefore, it can be concluded that high-LET radiation can better overcome the radioresistance of GSLCs in comparison with low-LET irradiation. Ionizing radiation produces a broad spectrum of molecular lesions in DNA, including single-strand breaks, DSBs, and a great variety of base damages. DSBs are the most toxic form of DNA damage, because a single unrepaired DSB can lead to abnormal mitosis with losses of large fragments of DNA [23]. Further, it is generally accepted that high-LET radiation induces more serious DNA DSBs than low-LET radiation [11, 24]. In the current study, we demonstrated that high-LET radiation could damage GSLCs that were resistant to low-LET gamma rays. As previously described, GSCs have a large capacity to repair DSBs induced by low-LET radiation [5]. However, it was uncertain whether or not high-LET radiation could cause serious DSBs that were unrepairable, even in GSCs.

To clarify the response to DNA DSBs induced by gamma rays or neutron beams, we employed a gamma-H2AX assay. From a previous report, we judged the persistence of gamma-H2AX foci 24 h after treatment as unrepairable DSB [25]. GSLCs had a larger restoration capacity for DSBs than CCs after low-LET radiation, but could not repair DSBs sufficiently after high-LET radiation (Fig. 4A and B). Because reduced survival was accompanied by the persistence of DNA damage, as evidenced by the persistence of gamma-H2AX foci after irradiation [26], high-LET radiation could produce persistence of DSBs and induce fatal damage even

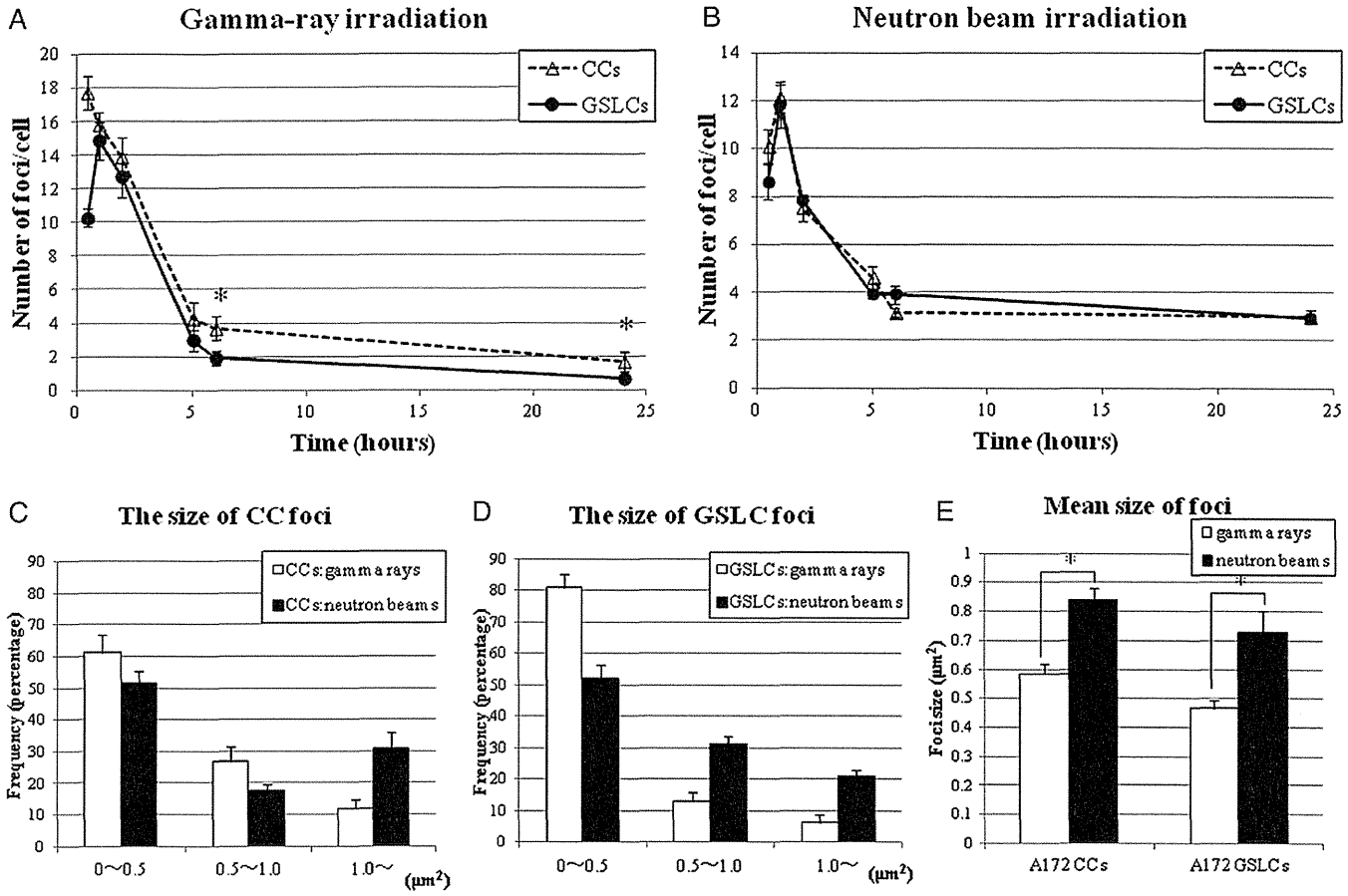

Fig. 4. Change in the number of induced nuclear gamma-H2AX foci and the histograms of gamma-H2AX foci size, at the times indicated post-irradiation in A172. These cells were irradiated with different types of beams (total physical dose = 4 Gy). (**A**) and (**B**) The numbers of gamma-H2AX foci per cell of GSLCs and CCs in A172 after the different types of radiation. (**C**) and (**D**) Distribution of gamma-H2AX foci sizes for A172 at 24 h post-irradiation. (**E**) Mean gamma-H2AX foci size for each type of A172 cells at 24 h post-irradiation. Bars represent the standard errors. $^*P < 0.05$ compared with gamma-H2AX foci per cell in GSLCs and CCs. GSLCs = glioma stem-like cells; CCs = control cells.

in GSLCs. In fact, it has been reported that to evaluate gamma-H2AX foci in cells exposed to high-LET radiation, the size of the foci should be considered, since high-LET radiation can cause larger gamma-H2AX foci than low-LET radiation [11, 27]. We therefore investigated not only the numbers of foci but also their size after 24 h irradiation by both types of radiation, and found that high-LET radiation could cause larger gamma-H2AX foci than low-LET radiation in both GSLCs and CCs (Figs. 3, 4C, 4D and 4E). As Fig. 4E shows, high-LET radiation led to significantly larger gamma-H2AX foci than low-LET radiation did, in both GSLCs and CCs. Therefore, it is thought that high-LET radiation could cause more serious DNA DSBs than low-LET radiation, even in GSLCs. In the previous report [28], low-LET irradiation might produce relatively large foci with time. In our experiment we demonstrated that high-LET particles produce larger foci in GSLC than low-LET gamma rays.

Indeed, under both gamma-ray and neutron-beam irradiation, more than half of all gamma-H2AX foci were small (0–0.5 μm^2). It is speculated that the neutron beams from KUR formed a wide-range beam that included gamma rays and secondary gamma rays. At the absorbed dose of 4 Gy, the compositions of fast, epithermal and thermal neutrons as well as of gamma rays were 25.5%, 2.5%, 22% and 50%, respectively. Almost half of the neutron beam components of the absorbed dose were induced by gamma rays, which could explain why small foci were induced mainly by gamma rays, even under neutron-beam irradiation. As described above, Fig. 3 also shows that the fluorescence intensity of gamma-H2AX foci after neutron irradiation was higher than that after gamma-ray irradiation. This may explain why high-LET radiation causes more intense DNA damage than low-LET radiation. A previous study showed that high-LET radiation, such as that from heavy ion therapy, had several potential advantages over low-LET radiation due to its induction of complex DNA damage that was not easily repaired [29], and may have an advantage over low-LET radiation for cancer stem-like cells [30]. Thus, our data also support the potential for use of high-LET radiation for GSCs.

Heavy ion treatment and BNCT are recognized as forms of high-LET radiation. In a previous report, when chemo-irradiation was combined with carbon ion therapy, the median survival time of GBM patients was 17 months [31]. In another report, BNCT followed by X-ray radiation therapy led to a median survival time of GBM patients of 21.3 months, even without chemotherapy [9]. Although both of these reports involved small numbers of patients, the results suggested that, since these high-LET radiations were effective even for GSCs in a clinical setting, patients could show prolonged survival. At the moment these treatment modalities are still at the clinical trial stage, but they may improve the standard treatment for GBM.

Although various treatments for GBM have been tried, an unfavorable prognosis can be expected with the current standard treatment. In the present study, we demonstrated that high-LET radiation may be able to overcome GSC resistance to low-LET radiation. It is necessary to further investigate the usefulness of high-LET radiation for the control of GSCs. High-LET radiation therapies such as BNCT or heavy ion therapy have very important roles in further treatment for therapy-resistant GBM.

CONFLICT OF INTEREST

The authors have no conflicts of interest to disclose.

FUNDING

This work was supported by a Grant-in-Aid for Scientific Research (B) (23390355) from the Japanese Ministry of Education, Culture, Sports, Science and Technology to S-IM.

REFERENCES

1. Stupp R, Mason WP, van den Bent MJ *et al.* Radiotherapy plus concomitant and adjuvant temozolomide for glioblastoma. *N Engl J Med* 2005;**352**:987–96.
2. Singh SK, Clarke ID, Terasaki M *et al.* Identification of a cancer stem cell in human brain tumors. *Cancer Res* 2003;**63**: 5821–8.
3. Singh SK, Hawkins C, Clarke ID *et al.* Identification of human brain tumour initiating cells. *Nature* 2004;**432**:396–401.
4. Yuan X, Curtin J, Xiong Y *et al.* Isolation of cancer stem cells from adult glioblastoma multiforme. *Oncogene* 2004;**23**: 9392–400.
5. Bao S, Wu Q, McLendon RE *et al.* Glioma stem cells promote radioresistance by preferential activation of the DNA damage response. *Nature* 2006;**444**:756–60.
6. Chang CJ, Hsu CC, Yung MC *et al.* Enhanced radiosensitivity and radiation-induced apoptosis in glioma CD133-positive cells by knockdown of SirT1 expression. *Biochem Biophys Res Commun* 2009;**380**:236–42.
7. Miyatake S, Kawabata S, Kajimoto Y *et al.* Modified boron neutron capture therapy for malignant gliomas performed using epithermal neutron and two boron compounds with different accumulation mechanisms: an efficacy study based on findings on neuroimages. *J Neurosurg* 2005;**103**:1000–9.
8. Miyatake S, Tamura Y, Kawabata S *et al.* Boron neutron capture therapy for malignant tumors related to meningiomas. *Neurosurgery* 2007;**61**:82–90; discussion 90–1.
9. Kawabata S, Miyatake S, Kuroiwa T *et al.* Boron neutron capture therapy for newly diagnosed glioblastoma. *J Radiat Res* 2009;**50**:51–60.
10. Miyatake S, Kawabata S, Yokoyama K *et al.* Survival benefit of Boron neutron capture therapy for recurrent malignant gliomas. *J Neurooncol* 2009;**91**:199–206.
11. Kinashi Y, Takahashi S, Kashino G *et al.* DNA double-strand break induction in Ku80-deficient CHO cells following boron neutron capture reaction. *Radiat Oncol* 2011;**6**:106.
12. Qiang L, Yang Y, Ma YJ *et al.* Isolation and characterization of cancer stem like cells in human glioblastoma cell lines. *Cancer Lett* 2009;**279**:13–21.
13. Sakurai Y, Kobayashi T. Characteristics of the KUR Heavy Water Neutron Irradiation Facility as a neutron field with variable energy spectra. *Nucl Instrum Meth A* 2000;**453**:569–96.
14. Kobayashi T, Kanda K. Analytical calculation of boron-10 dosage in cell nucleus for neutron capture therapy. *Radiat Res* 1982;**91**:77–94.
15. Kitao K. A method for calculating the absorbed dose near interface from 10B(n, alpha)7Li reaction. *Radiat Res* 1975; **61**:304–15.
16. Ohnishi T, Mori E, Takahashi A. DNA double-strand breaks: their production, recognition, and repair in eukaryotes. *Mutat Res* 2009;**669**:8–12.
17. Fukaya R, Ohta S, Yamaguchi M *et al.* Isolation of cancer stem-like cells from a side population of a human glioblastoma cell line, SK-MG-1. *Cancer Lett* 2010;**291**:150–7.
18. Vescovi AL, Galli R, Reynolds BA. Brain tumour stem cells. *Nat Rev Cancer* 2006;**6**:425–36.
19. Baumann M, Krause M, Hill R. Exploring the role of cancer stem cells in radioresistance. *Nat Rev Cancer* 2008;**8**:545–54.
20. Baumann M, Krause M, Thames H *et al.* Cancer stem cells and radiotherapy. *Int J Radiat Biol* 2009;**85**:391–402.
21. Ogden AT, Waziri AE, Lochhead RA *et al.* Identification of A2B5+CD133– tumor-initiating cells in adult human gliomas. *Neurosurgery* 2008;**62**:505–14; pdiscussion 514–5.
22. Shimura T, Noma N, Oikawa T *et al.* Activation of the AKT/cyclin D1/Cdk4 survival signaling pathway in radioresistant cancer stem cells. *Oncogenesis* 2012;**1**:e12.
23. van Gent DC, Hoeijmakers JH, Kanaar R. Chromosomal stability and the DNA double-stranded break connection. *Nat Rev Genet* 2001;**2**:196–206.
24. Leatherbarrow EL, Harper JV, Cucinotta FA *et al.* Induction and quantification of gamma-H2AX foci following low and high LET-irradiation. *Int J Radiat Biol* 2006;**82**:111–8.
25. Schmid TE, Dollinger G, Beisker W *et al.* Differences in the kinetics of gamma-H2AX fluorescence decay after exposure to low and high LET radiation. *Int J Radiat Biol* 2010;**86**: 682–91.
26. Prevo R, Deutsch E, Sampson O *et al.* Class I PI3 kinase inhibition by the pyridinylfuranopyrimidine inhibitor PI-103 enhances tumor radiosensitivity. *Cancer Res* 2008;**68**:5915–23.
27. Ibanez IL, Bracalente C, Molinari BL *et al.* Induction and rejoining of DNA double strand breaks assessed by H2AX

phosphorylation in melanoma cells irradiated with proton and lithium beams. *Int J Radiat Oncol Biol Phys* 2009;**74**: 1226–35.
28. Yamauchi M, Oka Y, Yamamoto M *et al.* Growth of persistent foci of DNA damage checkpoint factors is essential for amplification of G1 checkpoint signaling. *DNA Repair (Amst)* 2008; **7**:405–17.
29. Okayasu R, Okada M, Okabe A *et al.* Repair of DNA damage induced by accelerated heavy ions in mammalian cells proficient and deficient in the non-homologous end-joining pathway. *Radiat Res* 2006;**165**:59–67.
30. Cui X, Oonishi K, Tsujii H *et al.* Effects of carbon ion beam on putative colon cancer stem cells and its comparison with X-rays. *Cancer Res* 2011;**71**:3676–87.
31. Mizoe JE, Tsujii H, Hasegawa A *et al.* Phase I/II clinical trial of carbon ion radiotherapy for malignant gliomas: combined X-ray radiotherapy, chemotherapy, and carbon ion radiotherapy. *Int J Radiat Oncol Biol Phys* 2007;**69**:390–6.

Miyata et al. Radiation Oncology 2014, 9:51
http://www.ro-journal.com/content/9/1/51

RADIATION ONCOLOGY

RESEARCH Open Access

The roles of platelet-derived growth factors and their receptors in brain radiation necrosis

Tomo Miyata[1], Taichiro Toho[1], Naosuke Nonoguchi[1], Motomasa Furuse[1], Hiroko Kuwabara[2], Erina Yoritsune[1], Shinji Kawabata[1], Toshihiko Kuroiwa[1] and Shin-Ichi Miyatake[1*]

Abstract

Background: Brain radiation necrosis (RN) occurring after radiotherapy is a serious complication. We and others have performed several treatments for RN, using anticoagulants, corticosteroids, surgical resection and bevacizumab. However, the mechanisms underlying RN have not yet been completely elucidated. For more than a decade, platelet-derived growth factors (PDGFs) and their receptors (PDGFRs) have been extensively studied in many biological processes. These proteins influence a wide range of biological responses and participate in many normal and pathological conditions. In this study, we demonstrated that PDGF isoforms (PDGF-A, B, C, and D) and PDGFRs (PDGFR-α and β) are involved in the pathogenesis of human brain RN. We speculated on their roles, with a focus on their potential involvement in angiogenesis and inflammation in RN.

Methods: Seven surgical specimens of RN, obtained from 2006 to 2013 at our department, were subjected to histopathological analyses and stained with hematoxylin and eosin. We qualitatively analyzed the protein expression of each isoform of PDGF by immunohistochemistry. We also examined their expression with double immunofluorescence.

Results: All PDGFs were expressed in macrophages, microglia, and endothelial cells in the boundary of the core of RN, namely, the perinecrotic area (PN), as well as in undamaged brain tissue (UB). PDGF-C, D and PDGFR-α were also expressed in reactive astrocytes in PN. PDGFs and PDGFR-α were scarcely detected in UB, but PDGFR-β was specifically expressed in endothelial cells not only in PN but also in UB.

Conclusions: PDGFs/PDGFRs play critical roles in angiogenesis and possibly in inflammation, and they contribute to the pathogenesis of RN, irrespective of the original tumor pathology and applied radiation modality. Treatments for the inhibition of PDGF-C, PDGF-D, and PDGFR-α may provide new approaches for the treatment of RN induced by common radiation therapies.

Keywords: Angiogenesis, Brain radiation necrosis, Inflammation, Platelet-derived growth factors, Platelet-derived growth factor receptors

Background

Higher radiation doses to tumors result in good local tumor control and improvement in overall survival. On the other hand, radiation necrosis (RN) in the brain occurring after radiotherapy for brain tumors as well as for head and neck cancers is a serious complication that decreases the quality of life in patients. The mechanisms underlying RN have not been completely elucidated. In a previous study we showed that RN specimens stained with hematoxylin and eosin (H&E) typically show marked angiogenesis, so-called telangiectasis, microbleeding, and interstitial edema, probably caused by leakage of plasma from leaky angiogenesis into the surrounding necrotic core—namely, the perinecrotic area (PN) [1].

We and others have applied several treatments for RN, such as anticoagulants, vitamin E, corticosteroids, and surgical resection [2-4]. The typical MRI of symptomatic RN from case 3 demonstrated rapid shrinkage of the perilesional edema after surgical treatment [see Additional file 1 and Table 1]. After surgical resection for the only

* Correspondence: neu070@poh.osaka-med.ac.jp
[1]Department of Neurosurgery, Osaka Medical College, 2-7 Daigaku-machi, Takatsuki City, Osaka 569-8686, Japan
Full list of author information is available at the end of the article

Table 1 Clinical features of patients with symptomatic radiation necrosis

Pt.	Age (y)	Sex	Original dis.	Radiation[a]	Resection area (lobe)	Duration[b]	Chemo
1	46	F	SCC.	XRT (60 Gy), BNCT (13.9 Gy-Eq)	Temporal	7	MTX
2	78	M	Sal. Duc. Ca.	XRT (60 Gy), BNCT (13.9 Gy-Eq)	Frontotemporal	20	-
3	18	M	GBM	XRT (IMRT) (74 Gy)	Parietal	37	-
4	63	F	GBM	XRT (24 Gy), BNCT (13 Gy-Eq)	Frontoparietal	4	-
5	34	M	GBM	XRT (24 Gy), BNCT (13 Gy-Eq)	Frontal	6	-
6	56	F	GBM	Proton + XRT (total 90 Gy)	Temporoparietal	10	ACNU
7	46	F	Ade. Ca.	XRT (30 Gy), SRS (55 Gy, 65 Gy)	Frontal	32	Herceptin

Pt, patient; *y,* year; *F,* female; *M,* male; *Original dis,* original disease; *SCC,* Squamous cell carcinoma; *Sal. Duc. Ca,* salivary ductal carcinoma; *GBM,* glioblastoma; *Ade. Ca,* adenocarcinoma; *XRT,* X-ray radiation treatment; *IMRT* ,intensity modulated radiation therapy; *BNCT,* boron neutron capture therapy; *Proton,* proton beam therapy; *MTX,* methotrexate; *ACNU,* nimustin; *Herceptin,* trastuzumab;
[a]In Pt. 1 and 2, the temporal lobe was included in the irradiation field and in Pt. 3, 4, 5, and 6, local radiation therapy was administered. Pt. 7 had received whole brain irradiation and received SRS twice. In BNCT, the presented dose is the peak point dose for the normal brain.
[b]Months between termination of the last radiotherapy and onset of symptoms caused by radiation necrosis.

enhanced lesion, the perilesional edema decreased rapidly compared with preoperative MRI. This rapid shrinkage of the perilesional edema after surgical treatment was also observed in other cases. In addition, bevacizumab, an antibody for vascular endothelial growth factor (VEGF), has recently shown promising effects on symptomatic brain RN and symptomatic pseudo-progression [5,6]. However, in some cases, treatment with bevacizumab was not sufficient to resolve RN. Some RN cases recurred as RN even after temporary remission by bevacizumab treatment [7].

Recent experiments have shown that demyelination and damage of the normal vasculatures and the appearance of abnormal vasculatures around necrotic foci are major issues in the development of RN [8,9]. In addition, we previously reported that hypoxia-inducible factor 1α (HIF-1α) and VEGF are key molecules in RN [1]. In a later study, we tried to determine whether not only HIF-1α and VEGF, but also proinflammatory cytokines such as IL-1α, IL-6, TNF-α, and NFκB, might play significant roles in RN, since these cytokines were produced by CD68- and hGLUT5-positive microglia and/or macrophages accumulated in PN (in submission).

The platelet-derived growth factors (PDGFs) signaling pathway, which has been extensively studied and shown to play critical roles in many biological processes, is mediated through tyrosine kinase receptors (PDGFR-α, PDGFR-β) [10,11]. There are five members of the PDGF family: PDGF-A, B, and AB, and the recently discovered PDGF-C and D. So far, no heterodimers involving the PDGF-C and D chains have been described. PDGF-A binds only PDGFR-α, whereas PDGF-B activates PDGFR-α, αβ, and β. PDGF-A, B, and C activate PDGFR-α and αβ, while PDGF-D specifically binds to and activates its cognate receptor PDGFR-β. In other words, according to published data, PDGFR-α binds PDGF-A, B, AB, and C, whereas PDGFR-β binds PDGF-B and D [10,12,13].

In addition, PDGF-A and B are secreted in their active forms, while PDGF-C and D are secreted as inactive forms requiring activation for their function [14]. Interestingly, several reports have shown that the structure and biological function of PDGFs are quite similar to those of VEGF [15]. Therefore, the PDGF family is sometimes referred to as the VEGF family. Nevertheless, in recent years it was revealed that the angiogenic pathway induced by PDGF-C is, in large part, VEGF-independent [16].

Based on these findings, in this retrospective study we performed histopathological and immunohistochemical analyses on 7 human RN specimens from patients who we had treated surgically from 2006 to 2013 at our department. We here describe the findings common to all 7 of these specimens, and demonstrate which type of cells produce PDGFs and which type express the PDGFRs. We also evaluated the roles of PDGFs/PDGFRs in brain RN.

Methods

Case selection

Seven surgical specimens, obtained from 2006 to 2013, were submitted for histopathological analysis, staining with H&E, and immunohistochemistry. All the patients had received radiotherapy, including X-ray treatment (XRT), stereotactic radiosurgery (SRS), proton beam therapy, and boron neutron capture therapy (BNCT). The primary diseases were 4 glioblastomas, 2 head and neck cancers, and 1 metastatic brain tumor derived from breast cancer.

In this study we selected the area as radiation necrosis with extensive necrotic area with the boundary of extensive angiogenesis and edema, which is continuous to undamaged brain tissue, as mentioned in Background.

For the 2 patients with head and neck cancers, radiotherapy was used to treat the parotid lesions and the temporal lobe was included in the irradiation field. Therefore, there were no tumor cells in the brain, indicating pure brain RN. The patient characteristics are detailed in Table 1.

Histological and immunohistochemical staining

Histological and immunohistochemical analyses were performed on paraffin sections in which we observed the presence of RN by H&E staining. Each section was immunostained with the following antibodies: PDGF-A (1:20; R&D Systems, USA), PDGF-B (1:20; Abcam, Japan), PDGF-C (1:100; R&D Systems), PDGF-D (1:50; R&D Systems), PDGFR-α (1:20; R&D Systems), and PDGFR-β (1:50; R&D Systems) (Table 2). We routinely use a pressure cooker for 4 minutes to retrieve all the antigens. Endogenous peroxidase was blocked with 0.03% hydrogen peroxide for 40 minutes at room temperature. We used the ABC technique (Vector Laboratories, USA) for all of these antigens, before DAB (3, 3′ diaminobenzidine tetrahydrochloride (Wako Pure Chemical Industries, Japan)). The sections were counterstained with hematoxylin 3G (Sakura Finetek, Japan) and mounted.

Immunofluorescence

Double immunofluorescence was performed using the following antibody combinations: PDGF-C and GFAP (1:25; Dako, Denmark), CD68 (1:25; Epitomics, USA), hGLUT5 (1:50; IBL, Japan), or CD45 (1:50; Epitomics); PDGF-D and GFAP, CD68, hFLUT5, or CD45; PDGFR-α and GFAP, CD68, hGLUT5, or CD31 (1:20; Dako, Denmark); and PDGFR-β and GFAP, CD68, hGLUT5, or CD31.

GFAP, CD68, hGLUT5, CD45, and CD31 were adopted as markers for astrocytes, monocytes, microglia, lymphocytes, and endothelial cells, respectively. All sections were incubated with their respective antibodies for 24 hours with CD68, hGLUT5, and GFAP, and for 48 hours with PDGF-A, B, C, D, and PDGFR-α and β. Then, after washing the primary antibodies, Alexa Fluor 488 (1:25; Molecular Probes, USA) or Alexa Fluor 546 (1:25; Molecular Probes) was used (Table 3). Finally, the sections were examined using an LSM510 laser scanning confocal microscope (Carl Zeiss, Germany).

Table 2 List of primary antibodies used

Antibody	Clone	Sources	Type	Dilution
PDGF-A		R&D Systems, Minneapolis, MN	p/g	1:20
PDGF-B	MM0014-5 F66	Abcam Cambridge, MA	m/m	1:20
PDGF-C		R&D Systems, Minneapolis, MN	p/g	1:100
PDGF-D		R&D Systems, Minneapolis, MN	p/g	1:50
PDGFR-α		R&D Systems, Minneapolis, MN	p/g	1:20
PDGFR-β		R&D Systems, Minneapolis, MN	p/g	1:50
CD68	KP-1	Dako, Glostrup, Denmark	m/m	1:25
hGLUT5		IBL, Tokyo, Japan	p/r	1:50
GFAP	6 F2	Dako, Glostrup, Denmark	m/m	1:25
CD45	EP322Y	Eptomics, Burlingame, CA	m/r	1:50
CD31	JC70A	Dako, Glostrup, Denmark	m/m	1:20

p/g polyclonal goat; *p/r*, polyclonal rabbit; *m/r*, monoclonal rabbit; *m/m*, monoclonal mouse.

Statistical analysis

We assessed the frequency of expression of PDGFs semi-quantitatively by the following method. Five fields of each PDGF isoform in which abnormal angiogenesis was detected were randomly selected with a microscope. PDGF-positive mononuclear cells were counted. We observed 7 cases and, to reduce bias, used two observers to count the cells. One observer, who was blinded to the patients' clinical and pathological information, evaluated the results of immunohistochemical staining. The ratios of PDGF-positive cells per total cells in each field were calculated, and we statistically analyzed the data with Steel-Dwass tests using JMP Pro 10 (SAS Institute, USA). The results revealed that PDGF-C and D showed higher frequency of expression than PDGF-A and B in PN. The difference was statistically significant.

Ethical approval

This study was approved by an institutional committee of Osaka Medical College. The research was in compliance with the Helsinki Declaration.

Results

Expression of PDGFs

Figure 1 shows the results of H&E staining and immunohistochemistry from case 1. H&E staining revealed a necrotic

Table 3 Double immunofluorescence combinations

Primary	Dilution	Secondary	Primary	Dilution	Secondary
PDGF-C	1:50	F488	CD68	1:25	F546
PDGF-C	1:50	F488	hGLUT5	1:50	F546
PDGF-C	1:50	F488	GFAP	1:25	F546
PDGF-C	1:50	F488	CD45	1:50	F546
PDGF-D	1:20	F488	CD68	1:25	F546
PDGF-D	1:20	F488	hGLUT5	1:50	F546
PDGF-D	1:20	F488	GFAP	1:25	F546
PDGF-D	1:20	F488	CD45	1:50	F546
PDGFR-α	1:10	F488	CD68	1:25	F546
PDGFR-α	1:10	F488	hGLUT5	1:50	F546
PDGFR-α	1:10	F488	GFAP	1:25	F546
PDGFR-α	1:10	F488	CD31	1:20	F546
PDGFR-β	1:20	F488	CD68	1:25	F546
PDGFR-β	1:20	F488	hGLUT5	1:50	F546
PDGFR-β	1:20	F488	GFAP	1:25	F546
PDGFR-β	1:20	F488	CD31	1:20	F546

Primary, primary antibody; *Secondary*, secondary antibody; *F488*, Alexa Fluor 488; *F546*, Alexa Fluor 546.

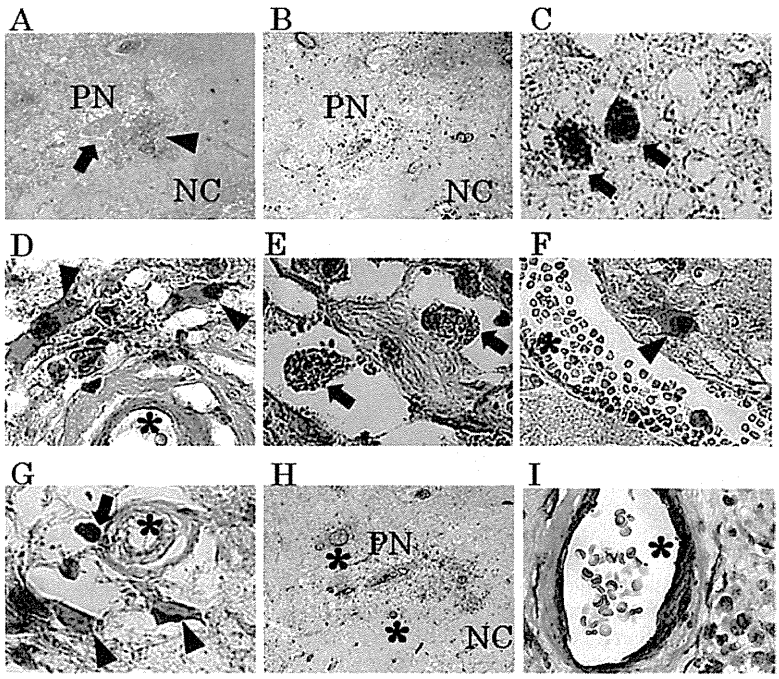

Figure 1 Results of hematoxylin and eosin staining (H&E) and immunohistochemistry from case 1. H&E staining **(A)** revealed a necrotic core (NC) and perinecrotic area (PN), including micro bleeding (**A**, arrowhead) and abnormal angiogenesis (**A**, arrow). Immunostaining results for PDGF-C are presented as a representative example **(B)**. PDGF-C **(C and D)**, **D (E and F)** and PDGFR-α **(G)** were produced by monocytic cells (**C**, **E**, **G**, arrow) and reactive astrocytic cells (**D**, **F**, **G**, arrowhead) in PN. On the other hand, PDGFR-β **(H and I)** was expressed mainly in endothelial cells **(H and I*)**. There was partially nonspecific staining in NC **(B)** or around blood vessels **(I)**. Original magnification, **A**, **B** and **H** × 40, **C**, **D**, **E**, **F**, **G** and **I** × 200.

core (NC) (Figure 1A. NC) and PN (Figure 1A. PN), in which micro bleeding (Figure 1A. arrowhead) and abnormal angiogenesis (Figure 1A. arrow) were confirmed. PDGF-A, B, C, and D-positive cells were detected in PN. The results of immunostaining for PDGF-C are shown as a typical example of these distribution analyses (Figure 1B, C, D). Morphologically, PDGF-A and B were produced by some monocytic cells [see Additional file 2] in PN. On the other hand, PDGF-C and D (Figure 1E, F) were produced by many monocytic cells (arrows in Figure 1C, E), reactive astrocytic cells (arrowheads in Figure 1D, F), and endothelial cells (Figure 1D*). PDGF-A, B, C, and D were scarcely detectable in UB (Figure 2).

These relationships among the expression of PDGFs are summarized in Table 4. These relationships were also confirmed with other specimens [see Additional file 3].

Our statistical analysis revealed that PDGF-C and D showed higher frequencies of expression than PDGF-A and B in PN. The difference was statistically significant ($p < 0.0001$, Steel-Dwass test) (Figure 3). We also grouped the cases into a GBM group (cases 3, 4, 5, 6) and non-GBM group (cases 1, 2, 7) and analyzed the differences in protein expression between them. No statistically significant differences in the expression of any of the isoforms were observed between the two groups by the Steel-Dwass test [see Additional file 4]. Therefore, we considered that these primary diseases did not affect the expression of PDGFs.

Double immunofluorescence from case 1 revealed that PDGF-C or D-positive cells were merged with many cells positive for CD68 (Figure 4A, E), GFAP (Figure 4B, F), hGLUT5 (Figure 4C, G), and CD45 (Figure 4D, H).

H&E staining, immunohistochemistry, and double immunofluorescence also showed similar tendencies in other specimens with symptomatic RN [see Additional files 3, and 5].

Expression of PDGFRs

PDGFR-α was expressed in endothelial cells (Figure 1G*), monocytic cells (Figure 1G arrow), and reactive astrocytic cells (Figure 1G, arrowhead) in PN. PDGFR-β was expressed mainly in endothelial cells (Figure 1H, I*). PDGFR-α was not expressed in any types of cells in UB (Figure 2E), but PDGFR-β was detected in endothelial cells in both PN and UB (Figure 2F).

Double immunofluorescence revealed that PDGFR-α and β were strongly expressed in CD31-positive cells (Figure 5D, I). PDGFR-β-positive cells were merged specifically with endothelial cells (Figure 5F, G, H, I and J, *), but PDGFR-α-positive cells were merged with cells positive for CD68 (Figure 5A), GFAP (Figure 5B), hGLUT5 (Figure 5C), and CD45 (Figure 5E) in PN.

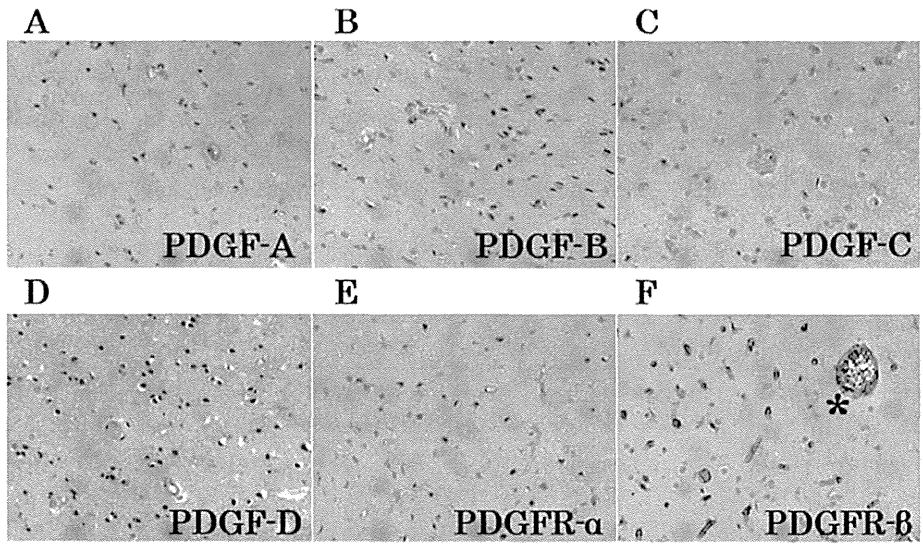

Figure 2 Representative results of immunostaining of undamaged brain tissue (UB). PDGF-A, B, C, D and PDGFR-α were scarcely detectable in UB **(A through E)**. PDGFR-β **(F)** was specifically expressed in endothelial cells in UB. Many normal cerebral blood vessels stained with PDGFR-β **(F *)** were detected in UB. Original magnification, ×200.

These findings from case 1 were confirmed in other specimens with symptomatic RN [see Additional file 6].

Double immunofluorescence revealed partially non-specific staining, especially in endothelial cells (Figures 4, and 5*). In cases where immunofluorescence was performed with GFAP alone, vascular endothelial cells were not stained [see Additional file 7]. These findings were also observed in other specimens.

Discussion

PDGFs are a group of multifunctional proteins with a wide variety of effects. They have important physiologic functions in embryonic and organ development, have been implicated in a wide variety of pathological processes, including proliferation, differentiation, and fibrogenesis, and are essential for the stability of normal blood vessel formation [16-19]. However, the overexpression of

Table 4 Expression of PDGFs/PDGFRs in two areas of the brain

	UB			PN		
	Mono	Astro	Endo	Mono	Astro	Endo
PDGF-A	-	-	-	+	-	+
PDGF-B	-	-	-	+	-	+
PDGF-C	-	-	-	+	+	+
PDGF-D	-	-	-	+	+	+
PDGFR-α	-	-	-	+	+	+
PDGFR-β	-	-	+	-	-	+

UB, undamaged brain area; *PN*, perinecrotic area; *Mono*, monocytes, including macrophages, microglia and lymphocytes *Astro*, reactive astrocytes; *Endo*, endothelial cells ; -, not expressed; +, expressed.

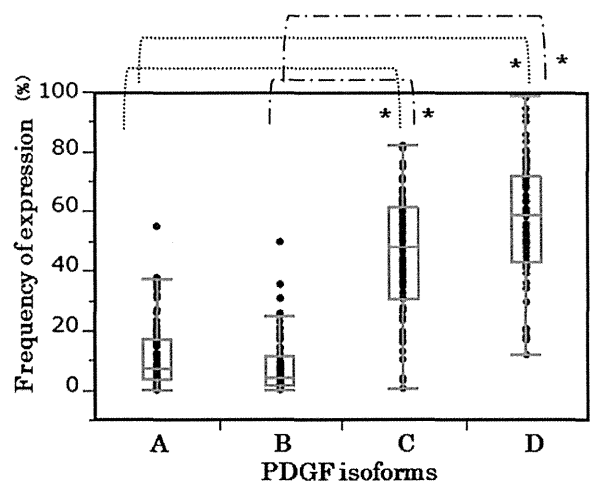

Figure 3 Frequency of expression. We assessed the frequency of expression of PDGFs semi-quantitatively by the following method. Five fields of each PDGF isoform, in which abnormal angiogenesis were detected, were randomly selected with a microscope. The PDGF-positive mononuclear cells were counted. We observed all 7 cases and performed the counting using two observers to reduce bias. One observer, who was blind to the patients' clinical and pathological information, evaluated the results of the immunohistochemical staining. The ratios of PDGF-positive cells to total cells in each field were calculated and were statistically analyzed using Steel-Dwass tests with JMP Pro 10 (SAS Institute Inc., Cary, NC, USA). Statistical analysis revealed that PDGF-C and D showed higher frequency of expression in the PN specimens than did PDGF-A and B. The difference was statistically significant (*$p < 0.0001$, Steel-Dwass test).

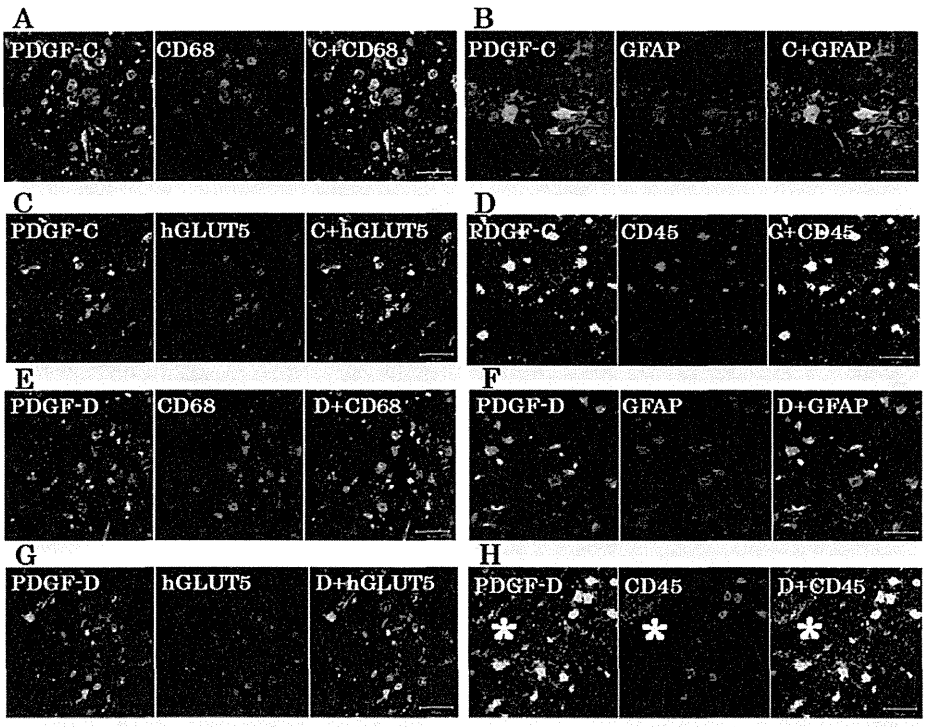

Figure 4 Double immunofluorescence staining. The results of double immunofluorescence staining from case 1 revealed that PDGF-C or D-positive cells were merged with many CD68 **(A, E)**, GFAP **(B, F)**, hGLUT5 **(C, G)**, and CD45 **(D, H)** -positive cells in PN. Some PDGF-C or D-positive cells did not express CD68, GFAP, hGLUT5 or CD45 and vice versa. Endothelial cells **(*)** were nonspecifically stained with secondary fluorescence antibody. The scale bar represents 50 μm.

PDGFs has adverse effects. Previous studies also have demonstrated that various cell types, including macrophages, fibroblasts, pericytes, and capillary endothelial cells, express PDGFs [20,21]. Deuel et al. also reported that a macrophage-derived PDGF induces chemotaxis and the proliferation of monocytes and fibroblasts during inflammation and wound repair [22].

This is the first study to explore the expression of PDGF isoforms and PDGFRs in human brain RN. Our results have shown that all PDGFs and PDGFRs were expressed in brain RN, and that PDGFs and PDGFRα were primarily expressed by macrophages, microglia, reactive astrocytes, lymphocytes, and endothelial cells in PN. These findings suggest that the activation of PDGFs is coincident with inflammation, angiogenesis, and fibrogenesis in the pathophysiology of RN.

Our recent study revealed that CD45-positive lymphocytes expressing CXCR4 might be drawn into PN from peripheral blood by chemotaxis, but they do not express proinflammatory cytokines, and their roles in RN remain unclear (submitted for publication). However, in the present study, CD45-positive lymphocytes produced PDGF-C and -D. These results suggest that CD45-positive lymphocytes in PN do not produce proinflammatory cytokines but may play significant indirect roles in angiogenesis and/or inflammation.

The highest differences of expression among PDGFs on brain RN were observed in PDGF-C and D (Figure 3 and Additional file 4). In this study, the expressions of PDGF-C and D were significantly higher than the expressions of PDGF-A and B in PN. Our current immunohistochemical study has further revealed that inflammatory cells, including macrophages, microglia, and even lymphocytes, were gathered in PN and produced PDGF-C and D. These mononuclear cells are known to play important roles in wound healing and inflammatory disease by producing a variety of growth factors and cytokines [23,24]. In our recent study, these mononuclear cells produced inflammatory cytokines (IL-1α, IL-6, TNF-α, NFκB) (submitted for publication). In the present study, these cells also produced PDGF-C and D. Therefore the activation of PDGF-C and D is coincident with inflammation as well as angiogenesis. These findings suggest that PDGF-C and D are involved in multiple aspects of brain RN.

The present and previous reports have revealed that the differential expression of PDGFs has also been seen in pathological conditions other than RN. In the aortic ring outgrowth assay, PDGF-C mediated significantly increased outgrowth, comparable to the levels mediated by VEGF and PDGF-A and B [25]. The angiogenic activity of PDGF-C in vivo is more potent than that of PDGF-A, AB or B [26]. PDGF-D also has been shown to stimulate

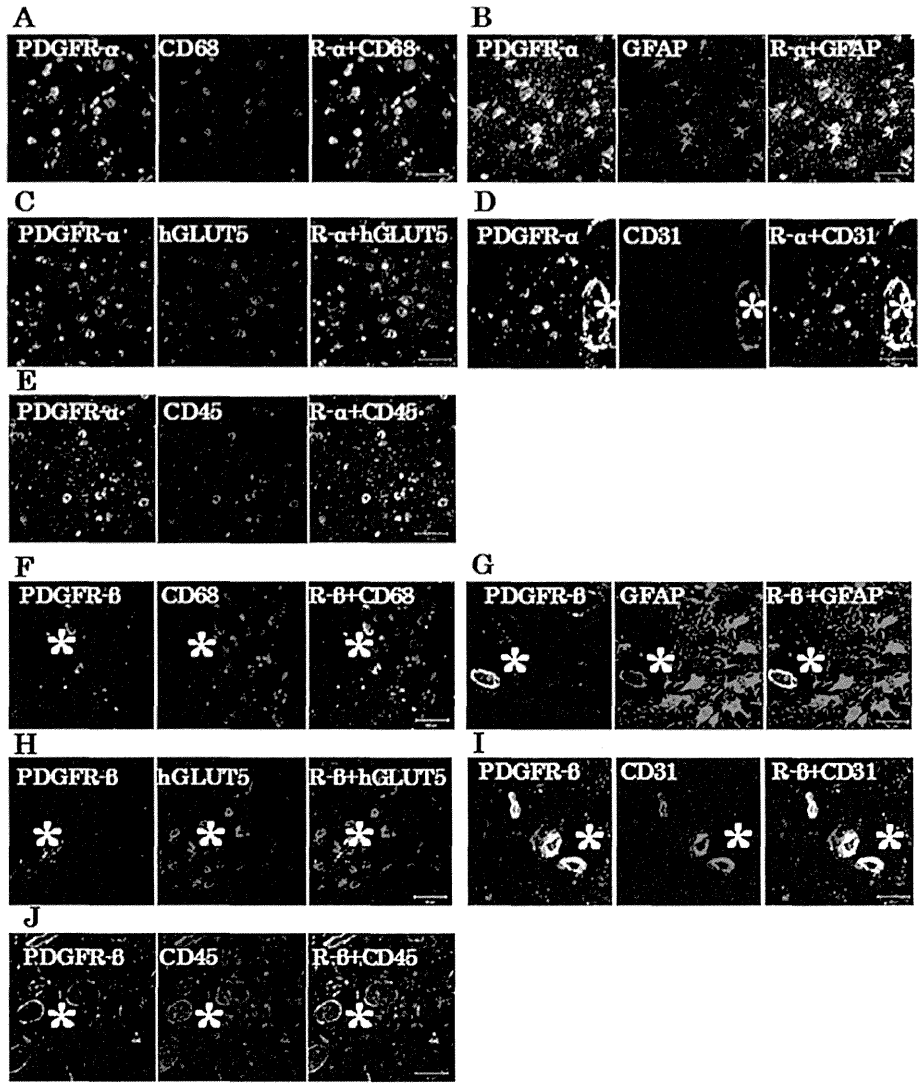

Figure 5 Double immunofluorescence staining. Double immunofluorescence staining from case 1 revealed that PDGFR-α and β were strongly expressed in CD31-positive cells in PN **(D and I)**. PDGFR-α positive cells were merged with many cells positive for CD68 **(A)**, GFAP **(B)**, hGLUT5 **(C)**, and CD45 **(E)**. PDGFR-β-positive cells merged specifically with endothelial cells **(F, G, H, I and J, *)**. Endothelial cells **(*)** were nonspecifically stained with secondary fluorescence antibody. The scale bar represents 50 μm.

angiogenesis and to play a critical role in wound healing [21,27,28].

Li et al. found that PDGF-D is a potent transforming and angiogenic growth factor for NIH/3 T3 cells, and that the transformed cells also induce VEGF expression [28]. Zhao et al. also found that inhibition of PDGF-D leads to decreased cell invasion in gastric cancer, partly through the regulation of VEGF [29]. In our study, many reactive astrocytes produced PDGF-C and D and expressed PDGFR-α, but these cells did not express PDGFR-β. These results established that PDGF-C and D play roles in angiogenesis and inflammation through autocrine and paracrine stimulation. Although the functions of these isoforms of PDGFs on cells are similar in many respects, each isoform might play different roles in different cell types via various receptors and pathways.

Previously, it was reported that several types of cells participate in angiogenesis and inflammation in brain RN [1,5,6]. But the underlying mechanisms have not been completely elucidated. We desperately need to know why different types of cells, including macrophages, microglia, lymphocytes, and astrocytes, acquire the capacity for differentiation, producing inflammatory cytokines and growth factors under certain pathological conditions. Ungvari et al. reported that γ-irradiated cerebromicrovascular endothelial cells acquired a senescence-associated secretory phenotype (SASP) characterized by the upregulation of proinflammatory cytokines and chemokines [30].

Our results suggest that several types of cells that survived irradiation in PN acquired SASP, and that this mechanism may be a key process in brain RN.

In this study, we performed retrospective analysis with clinical specimens of symptomatic RN and revealed that PDGFs/PSGFRs were involved in RN. However, this analysis covers just one aspect of RN. It is impossible to determine whether PDGFs exacerbate RN or rather are produced as a byproduct of RN. Also, we cannot speculate as to the dose–response relationship or the time course of the expression of PDGFs and their receptors in RN. These questions will be answered if a reproducible animal model of RN can be established.

Conclusions

In conclusion, PDGFs/PDGFRs play critical roles in angiogenesis and possibly in inflammation, and they contribute to the pathogenesis of RN, irrespective of the original tumor pathology and applied radiation modality. Moreover, the autocrine or paracrine signaling of PDGFs also plays crucial roles in aggressive angiogenesis and inflammation in RN. PDGF-C, PDGF-D and PDGFR-α have clinical importance, because PDGFR-β was expressed even in UB. Treatments to inhibit PDGF-C and D, or to inhibit PDGF-C and D in combination with PDGFR-α with a kinase inhibitor, may provide new approaches for RN induced by common radiation therapies, including XRT, SRS and BNCT.

Additional files

Additional file 1: Typical MRI of symptomatic radiation necrosis from case 3. Gd-enhanced T1 MRI just prior to excision of necrotic foci (A). Gd-enhanced T1 MRI 2 weeks after surgery (A'). FLAIR MRI just prior to excision of necrotic foci (B). FLAIR MRI, 2 weeks after surgery (B'). After surgical resection of the only enhanced lesion, perilesional edema was decreased compared with preoperative MRI.

Additional file 2: Representative immunohistochemistry from case 1. Immunostaining revealed the necrotic core (A, D NC) and perinecrotic area (A, D PN). PDGF-A (A, B, C) and PDGF-B (D, E) were produced by some monocytic cells (B, E arrow) and endothelial cells (C, E*) in PN. Original magnification, A, D × 40, B, C, E × 200.

Additional file 3: H&E staining and immunohistochemistry from case 3. H&E staining (A) and immunohistochemistry (B through O) from case 3, showing NC and PN. PDGF-A (B, C) and PDGF-B (D, E) were produced by some monocytic cells (arrows in C, E) in PN. In contrast, PDGF-C (F, G, H) and PDGF-D (I, J) were produced by many monocytic cells (arrows in G, H, J), reactive astrocytic cells (arrowheads in G, J), and endothelial cells (H, J*). PDGFR-α (K, L, M) was expressed in monocytic cells (L, arrow), reactive astrocytic cells (L, arrowhead) and endothelial cells (M*) in PN. PDGFR-β (N, O) was expressed mainly in endothelial cells (O*). Original magnification, A, B, D, F, I, K, N × 40, C, E, G, H, J, L, M, O × 200.

Additional file 4: Frequency of expression of PDGFs in the GBM group and non-GBM group. We assessed the frequency of expression of PDGFs semi-quantitatively. In the GBM group (cases 3, 4, 5, 6) and non-GBM group (cases 1, 2, 7), there was no apparent statistical significance in expression of each isoform (A, B, C, D).

Additional file 5: Double immunofluorescence staining results from case 3. Double immunofluorescence staining from case 3 revealed that PDGF-C or D-positive cells were merged with many CD68, hGLUT5, CD45 and GFAP-positive cells. Endothelial cells (*) were nonspecifically stained with secondary fluorescence antibody. The scale bar represents 50 μm.

Additional file 6: Double immunofluorescence staining results from case 3. Double immunofluorescence staining of the specimen from case 3 revealed that PDGFR-α and β were strongly expressed in CD31-positive cells (D and I). PDGFR-α-positive cells were merged with many cells positive for CD68 (A), GFAP (B), hGLUT5 (C), and CD45 (E). PDGFR-β-positive cells were merged specifically with endothelial cells (F thorough J). Endothelial cells (*) were nonspecifically stained with secondary fluorescence antibody. The scale bar represents 50 μm.

Additional file 7: Immunofluorescence staining from consecutive specimens from case 1 and 3. Immunofluorescence staining of consecutive specimens from case 1 (A, B) and 3 (C, D) showed positivity for PDGFR-β (A) or GFAP (B). PDGFR-β (A) was not observable at an excitation wavelength of 561 nm but was apparent at 499 nm in endothelial cells (*). On the other hand, GFAP (B) was observed only at an excitation wavelength of 561 nm in reactive astrocytes. The scale bar represents 50 μm.

Abbreviations

RN: Radiation necrosis; PDGFs: Platelet-derived growth factors; PDGFRs: Platelet-derived growth factor receptors; H&E: Hematoxylin and eosin; PN: Perinecrotic area; UB: Undamaged brain tissue; VEGF: Vascular endothelial growth factor; HIF-1α: Hypoxia-inducible factor 1α; XRT: X-ray treatment; SRS: Stereotactic radiosurgery; Proton: Proton beam therapy; BNCT: Boron neutron capture therapy; NC: Necrotic core; SASP: Senescence-associated secretory phenotype; CTLs: Cytotoxic T-lymphocytes.

Competing interests

The authors declare that they have no competing interests.

Authors' contributions

TM carried out the statistical analysis and drafted the manuscript. S-IM conceived of the study, participated in its design and coordination, and helped to draft the manuscript. TT, NN, MF, HK, EY, SK, and TK participated in the study design and coordination and helped to draft the manuscript. All authors read and approved the final manuscript.

Acknowledgments

This work was partly supported by a Grant-in-Aid for Scientific Research (B) (23390355) and by a Grant-in-Aid for Exploratory Research (24659658) to S-I. M. and by a Grant-in-Aid for Scientific Research (C) (23592145) to M.F. from the Japanese Ministry of Education, Culture, Sports, Science, and Technology. We thank Itsuko Inoue and Kaname Shimokawa for their technical assistance.

Author details

[1]Department of Neurosurgery, Osaka Medical College, 2-7 Daigaku-machi, Takatsuki City, Osaka 569-8686, Japan. [2]Department of Pathology, Osaka Medical College, 2-7 Daigaku-machi, Takatsuki City, Osaka 569-8686, Japan.

Received: 15 October 2013 Accepted: 3 February 2014
Published: 11 February 2014

References

1. Nonoguchi N, Miyatake S, Fukumoto M, Furuse M, Hiramatsu R, Kawabata S, Kuroiwa T, Tsuji M, Ono K: **The distribution of vascular endothelial growth factor-producing cells in clinical radiation necrosis of the brain: pathological consideration of their potential roles.** *J Neurooncol* 2011, 105:423–431.
2. Giglio P, Gilbert MR: **Cerebral radiation necrosis.** *Neurologist* 2003, 9:180–188.
3. Glantz MJ, Burger PC, Friedman AH, Radtke RA, Massey EW, Schold SC Jr: **Treatment of radiation-induced nervous system injury with heparin and warfarin.** *Neurology* 1994, 44:2020–2027.
4. Levin VA, Bidaut L, Hou P, Kumar AJ, Wefel JS, Bekele BN, Grewal J, Prabhu S, Loghin M, Gilbert MR, Jackson EF: **Randomized double-blind placebo-controlled trial of bevacizumab therapy for radiation necrosis of the central nervous system.** *Int J Radiat Oncol Biol Phys* 2011, 79:1487–1495.

5. Furuse M, Nonoguchi N, Kawabata S, Yoritsune E, Takahashi M, Inomata T, Kuroiwa T, Miyatake S: **Bevacizumab treatment for symptomatic radiation necrosis diagnosed by amino acid PET.** *Jpn J Clin Oncol* 2013, **43**:337–341.
6. Miyatake SI, Furuse M, Kawabata S, Maruyama T, Kumabe T, Kuroiwa T, Ono K: **Bevacizumab treatment of symptomatic pseudoprogression after boron neutron capture therapy for recurrent malignant gliomas. Report of 2 cases.** *Neuro-oncology* 2013, **15**:650–655.
7. Furuse M, Kawabata S, Kuroiwa T, Miyatake S: **Repeated treatments with bevacizumab for recurrent radiation necrosis in patients with malignant brain tumors: a report of 2 cases.** *J Neurooncol* 2011, **102**:471–475.
8. Arbab AS, Janic B, Jafari-Khouzani K, Iskander AS, Kumar S, Varma NR, Knight RA, Soltanian-Zadeh H, Brown SL, Frank JA: **Differentiation of glioma and radiation injury in rats using in vitro produce magnetically labeled cytotoxic T-cells and MRI.** *PLoS One* 2010, **5**:e9365.
9. Kumar S, Arbab AS, Jain R, Kim J, deCarvalho AC, Shankar A, Mikkelsen T, Brown SL: **Development of a novel animal model to differentiate radiation necrosis from tumor recurrence.** *J Neurooncol* 2012, **108**:411–420.
10. Heldin CH, Westermark B: **Mechanism of action and in vivo role of platelet-derived growth factor.** *Physiol Rev* 1999, **79**:1283–1316.
11. Heldin CH, Ostman A, Ronnstrand L: **Signal transduction via platelet-derived growth factor receptors.** *Biochim Biophys Acta* 1998, **1378**:F79–F113.
12. Bergsten E, Uutela M, Li X, Pietras K, Ostman A, Heldin CH, Alitalo K, Eriksson U: **PDGF-D is a specific, protease-activated ligand for the PDGF beta-receptor.** *Nat Cell Biol* 2001, **3**:512–516.
13. Li X, Ponten A, Aase K, Karlsson L, Abramsson A, Uutela M, Backstrom G, Hellstrom M, Bostrom H, Li H, *et al*: **PDGF-C is a new protease-activated ligand for the PDGF alpha-receptor.** *Nat Cell Biol* 2000, **2**:302–309.
14. Wang Z, Ahmad A, Li Y, Kong D, Azmi AS, Banerjee S, Sarkar FH: **Emerging roles of PDGF-D signaling pathway in tumor development and progression.** *Biochim Biophys Acta* 1806, **2010**:122–130.
15. Lei H, Kazlauskas A: **Focus on molecules: platelet-derived growth factor C, PDGF-C.** *Exp Eye Res* 2008, **86**:711–712.
16. Wang Z, Kong D, Banerjee S, Li Y, Adsay NV, Abbruzzese J, Sarkar FH: **Down-regulation of platelet-derived growth factor-D inhibits cell growth and angiogenesis through inactivation of Notch-1 and nuclear factor-kappaB signaling.** *Cancer Res* 2007, **67**:11377–11385.
17. Hoch RV, Soriano P: **Roles of PDGF in animal development.** *Development* 2003, **130**:4769–4784.
18. Li R, Maminishkis A, Wang FE, Miller SS: **PDGF-C and -D induced proliferation/migration of human RPE is abolished by inflammatory cytokines.** *Invest Ophthalmol Vis Sci* 2007, **48**:5722–5732.
19. Lindahl P, Johansson BR, Leveen P, Betsholtz C: **Pericyte loss and microaneurysm formation in PDGF-B-deficient mice.** *Science* 1997, **277**:242–245.
20. Li X, Kumar A, Zhang F, Lee C, Li Y, Tang Z, Arjuna P: **VEGF-independent angiogenic pathways induced by PDGF-C.** *Oncotarget* 2010, **1**:309–314.
21. Uutela M, Wirzenius M, Paavonen K, Rajantie I, He Y, Karpanen T, Lohela M, Wiig H, Salven P, Pajusola K, *et al*: **PDGF-D induces macrophage recruitment, increased interstitial pressure, and blood vessel maturation during angiogenesis.** *Blood* 2004, **104**:3198–3204.
22. Deuel TF, Senior RM, Huang JS, Griffin GL: **Chemotaxis of monocytes and neutrophils to platelet-derived growth factor.** *J Clin Invest* 1982, **69**:1046–1049.
23. Kumagai S, Ohtani H, Nagai T, Funa K, Hiwatashi N, Shimosegawa T, Nagura h: **Platelet-derived growth factor and its receptors are expressed in areas of both active inflammation and active fibrosis in inflammatory bowel disease.** *Tohoku J Exp Med* 2001, **195**:21–33.
24. Leibovich SJ, Ross R: **The role of the macrophage in wound repair. A study with hydrocortisone and antimacrophage serum.** *Am J Pathol* 1975, **78**:71–100.
25. Gilbertson DG, Duff ME, West JW, Kelly JD, Sheppard PO, Hofstrand PD, Gao Z, Shoemaker K, Bukowski TR, Moore M, *et al*: **Platelet-derived growth factor C (PDGF-C), a novel growth factor that binds to PDGF alpha and beta receptor.** *J Biol Chem* 2001, **276**:27406–27414.
26. Cao R, Brakenhielm E, Li X, Pietras K, Widenfalk J, Ostman A, Eriksson U, Cao Y: **Angiogenesis stimulated by PDGF-CC, a novel member in the PDGF family, involves activation of PDGFR-alphaalpha and -alphabeta receptors.** *FASEB J* 2002, **16**:1575–1583.
27. LaRochelle WJ, Jeffers M, Corvalan JR, Jia XC, Feng X, Vanegas S, Vickroy JD, Yang XD, Chen F, Gazit G, *et al*: **Platelet-derived growth factor D: tumorigenicity in mice and dysregulated expression in human cancer.** *Cancer Res* 2002, **62**:2468–2473.
28. Li H, Fredriksson L, Li X, Eriksson U: **PDGF-D is a potent transforming and angiogenic growth factor.** *Oncogene* 2003, **22**:1501–1510.
29. Zhao L, Zhang C, Liao G, Long J: **RNAi-mediated inhibition of PDGF-D leads to decreased cell growth, invasion and angiogenesis in the SGC-7901 gastric cancer xenograft model.** *Cancer Biol Ther* 2010, **9**:42–48.
30. Ungvari Z, Podlutsky A, Sosnowska D, Tucsek Z, Toth P, Deak F, Gautam T, Csiszar A, Sonntag WE: **Ionizing radiation promotes the acquisition of a senescence-associated secretory phenotype and impairs angiogenic capacity in cerebromicrovascular endothelial cells: role of increased DNA damage and decreased DNA repair capacity in microvascular radiosensitivity.** *J Gerontol Series A, Biol Sci Med Sci* 2013, **68**:1443–1457.

doi:10.1186/1748-717X-9-51
Cite this article as: Miyata *et al.*: The roles of platelet-derived growth factors and their receptors in brain radiation necrosis. *Radiation Oncology* 2014 9:51.

International Journal of
Radiation Oncology
biology • physics

www.redjournal.org

Clinical Investigation

Phase 2 Trial of Hypofractionated High-Dose Intensity Modulated Radiation Therapy With Concurrent and Adjuvant Temozolomide for Newly Diagnosed Glioblastoma

Toshihiko Iuchi, MD, PhD,* Kazuo Hatano, MD, PhD,† Takashi Kodama, PhD,† Tsukasa Sakaida, MD, PhD,* Sana Yokoi, MD, PhD,‡ Koichiro Kawasaki, MD,* Yuzo Hasegawa, MD, PhD,* and Ryusuke Hara, MD, PhD†

*Divisions of *Neurological Surgery, †Radiation Oncology, and ‡Gene Diagnosis, Chiba Cancer Center, Chiba, Japan*

Received Sep 14, 2013, and in revised form Dec 5, 2013. Accepted for publication Dec 10, 2013.

Summary

The clinical effect of hypofractionated high-dose intensity modulated radiation therapy with concurrent and adjuvant temozolomide was evaluated in 46 patients with glioblastomas. This treatment was performed without radiation-related adverse events and altered the dominant failure pattern from localized to disseminated. The median survival was 20.0 months. Radiation necrosis was the most frequently observed late toxicity, but necrosis in the subventricular zone was significantly associated with better survival.

Purpose/Objectives: To assess the effect and toxicity of hypofractionated high-dose intensity modulated radiation therapy (IMRT) with concurrent and adjuvant temozolomide (TMZ) in 46 patients with newly diagnosed glioblastoma multiforme (GBM).

Methods and Materials: All patients underwent postsurgical hypofractionated high-dose IMRT. Three layered planning target volumes (PTVs) were contoured. PTV1 was the surgical cavity and residual tumor on T1-weighted magnetic resonance images with 5-mm margins, PTV2 was the area with 15-mm margins surrounding the PTV1, and PTV3 was the high-intensity area on fluid-attenuated inversion recovery images. Irradiation was performed in 8 fractions at total doses of 68, 40, and 32 Gy for PTV1, PTV2, and PTV3, respectively. Concurrent TMZ was given at 75 mg/m^2/day for 42 consecutive days. Adjuvant TMZ was given at 150 to 200 mg/m^2/day for 5 days every 28 days. Overall and progression-free survivals were evaluated.

Results: No acute IMRT-related toxicity was observed. The dominant posttreatment failure pattern was dissemination. During a median follow-up time of 16.3 months (range, 4.3-80.8 months) for all patients and 23.7 months (range, 12.4-80.8 months) for living patients, the median overall survival was 20.0 months after treatment. Radiation necrosis was diagnosed in 20 patients and was observed not only in the high-dose field but also in the subventricular zone (SVZ). Necrosis in the SVZ was significantly correlated with prolonged survival (hazard ratio, 4.08; $P=.007$) but caused deterioration in the performance status of long-term survivors.

Conclusions: Hypofractionated high-dose IMRT with concurrent and adjuvant TMZ altered the dominant failure pattern from localized to disseminated and prolonged the survival of patients with GBM. Necrosis in the SVZ was associated with better patient survival, but the benefit of radiation to this area remains controversial. © 2014 Elsevier Inc.

Reprint requests to: Toshihiko Iuchi, MD, PhD, Division of Neurological Surgery, Chiba Cancer Center, 666-2 Nitona-cho, Chuo-ku, Chiba 260-8717, Japan. Tel: (81) 43-264-5431; E-mail: tiuchi@chiba-c.jp

Supported by a JSPS KAKENHI grant (grant no. 21591886).
Conflict of interest: none.

Int J Radiation Oncol Biol Phys, Vol. ■, No. ■, pp. 1–8, 2014
0360-3016/$ - see front matter
http://dx.doi.org/10.1016/j.ijrobp.2013.12.011

Introduction

Glioblastoma multiforme (GBM) is the most common primary malignant brain tumor. Surgical removal followed by radiation therapy with concurrent and adjuvant temozolomide (TMZ) is the standard treatment for newly diagnosed GBM. Although TMZ can improve patient outcomes, the prognosis remains poor, and the median survival is only 14.6 months after treatment (1).

The failure pattern after standard treatment is local (2), and intensive treatment targeting localized lesions is required to improve the outcome in patients with GBM. We initiated a phase 2 trial of hypofractionated high-dose intensity modulated radiation therapy (IMRT) with concurrent and adjuvant TMZ for better control of GBM in 2006. In the present study, we investigated the efficacy and safety of our intensive IMRT using TMZ in patients with GBM.

Methods and Materials

Patients

This single-institution prospective study was approved by the ethics committee of our institution. Eligibility criteria included newly diagnosed and pathologically confirmed GBM without an enhanced lesion beside the cerebrospinal fluid (CSF) space on baseline magnetic resonance imaging (MRI), age $\geq$18 years, and normal liver, kidney, and bone marrow function.

Surgical removal

Before registration, surgical tumor removal was performed in all patients. The extent of resection was not part of the inclusion criteria but was calculated by comparing preoperative and postoperative MRI. Gross total resection was defined as removal of $\geq$95% of the enhancing tumor.

The methylation status of the *O-6-methylguanine-DNA methyltransferase (MGMT)* gene promoter was determined by methylation-specific polymerase chain reaction analysis (3).

Hypofractionated high-dose IMRT

Computed tomography (CT) simulation with a 2-mm slice thickness was performed for all patients. MRIs of fluid-attenuated inversion recovery (FLAIR) images and contrast-enhanced T1-weighted images were also obtained before planning and were fused to the simulated CT images for target delineation. A simultaneous integrated boost technique was used to deliver different radiation doses to layered targets. The gross tumor volume (GTV) was defined as the contrast-enhancing residual tumor plus the entire surgical cavity on MRI. The planning target volume 1 (PTV1) was defined as the GTV plus a 5-mm margin, PTV2 as a 15-mm margin surrounding PTV1, and PTV3 as the high-intensity region on FLAIR images without margins. Irradiation was delivered in 8 fractions over 10 days (total dose of 68 Gy in 8.5-Gy fractions to PTV1, 40 Gy in 5.0-Gy fractions to PTV2, and 32 Gy in 4.0-Gy fractions to PTV3). IMRT was performed with either multiple static intensity-modulated beams or intensity-modulated dynamic arcs.

Concurrent and adjuvant chemotherapy

All patients underwent concurrent and adjuvant TMZ. This agent was administrated orally, once daily, at 75 mg/m^2 for 42 consecutive days. This treatment was begun within 1 week after registration, and IMRT was performed during this course of chemotherapy. Adjuvant TMZ was administered at 150 to 200 mg/m^2 orally, once daily, for 5 consecutive days every 28 days, for a total of 12 cycles or until tumor progression.

Patient follow-up

The failure patterns were classified as follows: local (at the regional tumor), distant (intraparenchymal, but distant from the original tumor site), and disseminated (distant from the original tumor and exposed to the CSF space) (Fig. 1). Contrast-enhanced MRI was performed within 14 days before IMRT to obtain baseline images, then at intervals of 1 or 2 months after IMRT. If an enhanced lesion appeared, C^{11}-methionine positron emission tomography (Met-PET) was performed, and the uptake of methionine was semiquantitatively evaluated by the ratio of uptake in the lesion to that in the contralateral normal brain (T/N ratio). Enhancing lesions with a T/N ratio of $>$1.8 were diagnosed as tumor progression, and lesions with a ratio of $\leq$1.8 were diagnosed as radiation necrosis. The lesion was diagnosed as tumor progression regardless of methionine uptake when viable cells were revealed in the specimen at the second surgery. When Met-PET was not available, daily dexamethasone was administered orally, and MRI was performed 4 to 8 weeks later. The lesion was diagnosed as necrosis when it shrunk on MRI but as recurrence in other cases.

Hematologic and nonhematologic toxicities were evaluated monthly. Toxicities were graded according to the Common Terminology Criteria for Adverse Events, version 4.0.

Statistical analysis

The primary endpoint of this study was overall survival (OS); the secondary endpoints were progression-free survival and safety. Survival curves were drawn by the Kaplan-Meier method, and a 2-sided log—rank test was used for analysis. Cox's proportional hazard model gave estimates for the hazard ratios (HRs). All analyses were performed on an intention-to-treat basis with JAMP software (version 10.0.2).

Results

Patients

Between August 2006 and August 2012, a total of 46 patients were enrolled in this study. Their median age was 65.5 years (range, 40-80 years), and 27 of the 46 patients (59%) were Radiation Therapy Oncology Group recursive partitioning analysis (RTOG RPA) class V or VI. The location of the tumor according to the classification of Lim et al (4) was as follows: group 1 in 18 patients, group 2 in 12, group 3 in 13, and group 4 in 3; the enhanced lesion contacted the subventricular zone (SVZ) in 30 patients (65%). The patient characteristics are summarized in Table 1.

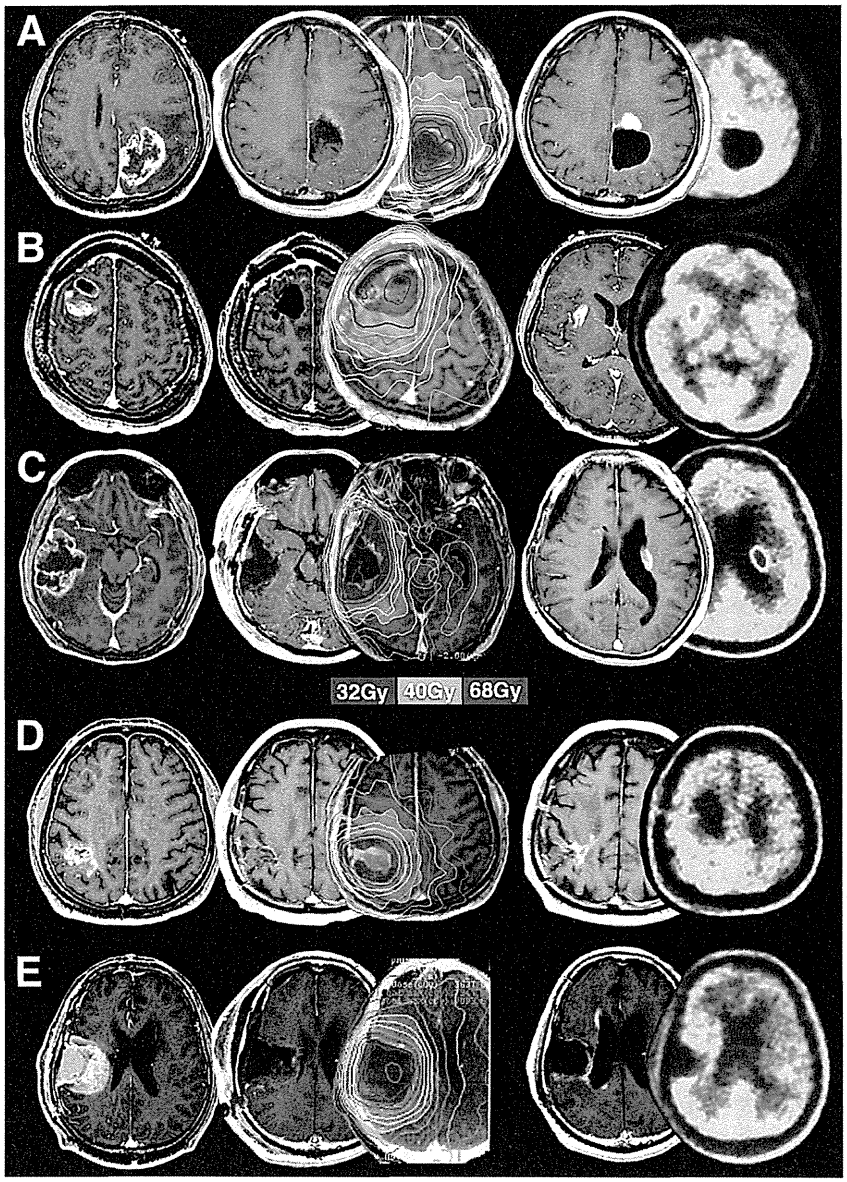

Fig. 1. Failure patterns and radiation necrosis patterns. Three different patterns of failure were evident: local (A), distant (B), and disseminated (C). Two different patterns of radiation necrosis were evident: regional necrosis (D) and necrosis in the subventricular zone (E). Enhanced magnetic resonance imaging (MRI) performed before (left) and after (middle) surgery and at the reappearance of enhanced lesions on MRI was demonstrated with isodose maps and methionine-positron emission tomography.

At the time of the last follow-up visits, the median follow-up periods were 16.3 months (range, 4.3-80.8 months) for all patients and 23.7 months (range, 12.4-80.8 months) for living patients.

Hypofractionated high-dose IMRT

All patients were treated according to the protocol. The median PTV1 was 80.9 cc (range, 26.5-267.2 cc), the median PTV2 was 160.7 cc (range, 78.5-374.3 cc), and the median PTV3 was 0.6 cc (range, 0.0-65.9 cc).

Concurrent and adjuvant TMZ

Temozolomide was administered to all patients concurrently with IMRT but was withdrawn 12 days after initiation in 1 patient because of a grade 3 skin rash. In addition to this patient, adjuvant chemotherapy was abundant in 4 patients because of adverse events of TMZ: grade 3 pneumonitis in 1, grade 3 fatigue in 2, and grade 3 bone marrow suppression in 1. In addition to those 5 patients, TMZ was discontinued in 5 patients because of performance status deterioration. Among the remaining 36 patients, 12 cycles of TMZ were completed without tumor progression in 13

Table 1 Patient characteristics (N=46)

Characteristics	n
Age, y	
<60/≤60	14/32
Sex	
Female/Male	16/30
KPS (%)	
<70/≤70	23/23
Extent of resection	
<95%/≤95%	17/29
RPA class	
III/IV/V/VI	2/17/16/11
MGMT	
Met/UnMet	11/34*

Abbreviations: KPS = Karnofsky performance status; Met = methylated; MGMT = *O-6-methylguanine-DNA methyltransferase* gene; RPA = recursive partitioning analysis; UnMet = unmethlylated.
* *MGMT* methylation status was not available in 1 case.

patients, but TMZ was withdrawn because of tumor progression in 23. The median number of TMZ cycles was 5.

Local control

Progression of enhancing lesions at the original tumor site was observed in 19 patients. Among these lesions, 13 were diagnosed as tumor progression: high methionine uptake in 5 and continuous progression on MRI in 8. Removal of these lesions was performed in 9 patients, including 5 diagnosed by Met-PET, and a viable tumor was found in all patients. The remaining 6 lesions were diagnosed as necrosis because of low methionine uptake on PET images. Among these 6 patients, second surgery was performed in 1, and no viable cells were found. Pathologic evaluation was not available for the remaining 5 patients, but the enhanced lesion shrank on MRI by dexamethasone in all patients.

Among these 13 tumor progressions, 4 recurrences were diagnosed after diagnosis of other types of failures: after distant failure in 2 and after dissemination in 2.

The 2- and 5-year local progression-free survival was 63.9% and 57.5%, respectively (Fig. 2A). We found no clinical variables that were significantly associated with local lesion control.

Other types of failures

Distant failure was observed in 10 patients during the course of their disease (Fig. 2B). Half of these distant failures appeared after other types of failures, and distant failure was the primary failure pattern in 5 patients. No clinical variable significantly affected distant failure-free survival.

Dissemination was more common in our series. This type of failure was diagnosed in 21 patients and before other types of failure in 14 patients (Fig. 2C). These disseminated lesions were located at the lateral ventricle wall in 14 patients, surrounding the brain stem in 2, at the surface of the brain convexity in 2, in the fourth ventricle in 2, and in the spinal canal in 1. We found no clinical variables that were significantly associated with dissemination.

Consequently, the dominant failure pattern in our patients was dissemination: the primary site of failure was local in 11 patients, distant in 5, and beside the CSF space in 14. The median time to any type of failure was 9.7 months after treatment (Fig. 2D).

Survival

At the time of the last follow-up visits, 37 patients had died. The cause of death was disseminated disease progression in 15, local tumor progression in 9, distant lesion progression in 1, radiation

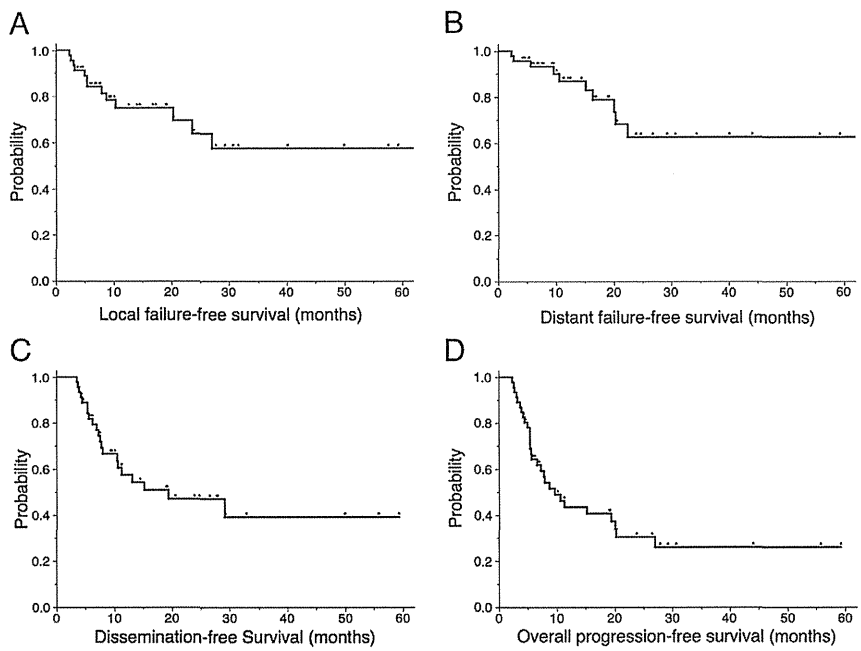

Fig. 2. Progression-free survival. The times to progression were analyzed differently according to the failure site: failure at the original tumor site (A), distant failure (B), and disseminated failure (C). The time to the first progression regardless of the pattern of failure was also demonstrated (D).